ELSEVIER

Pattern Recognition Letters 17 (1996) 1191-1198

Pattern Recognition Letters

Target indexing in SAR images using scattering centers and the Hausdorff distance

June Ho Yi, Bir Bhanu *, Ming Li

Visualization and Intelligent Systems Laboratory, College of Engineering, University of California, Riverside, CA 92521-0425, USA

Received 21 November 1995; revised 11 June 1996

Abstract

This paper is concerned with efficient and accurate indexing for target recognition in SAR images. We present a method that efficiently retrieves correct object hypotheses using the major axis of a pattern of scattering centers in SAR images and the Hausdorff distance measure. The features that we use are the locations of scattering centers in SAR returns. Experimental results show that indexing using major axis efficiently narrows down the number of candidate hypotheses and that the Hausdorff distance measure performs well in picking the correct hypothesis. These properties of the algorithm along with computational efficiency make our method a promising approach to target indexing in SAR images.

Keywords: SAR; Target recognition; Indexing

1. Introduction

Automatic target recognition (ATR) from synthetic aperture radar (SAR) imagery is an important aspect of current vision research. Some of the representative work in ATR from SAR images includes (Dudgeon et al., 1994; Novak et al., 1993; Waxman et al., 1993). This work focuses on template matching techniques in which the templates are manually designed. However, few research works on target indexing using SAR images have been reported in the literature. As compared to visible imagery, recognition of targets in SAR imagery (Special issue, 1993; Bhanu et al., 1996) is a very challenging and difficult task because of the non-literal nature of SAR images. One has to understand the physics of SAR image formation to interpret them (Fitch, 1988).

Indexing is one of the fundamental issues in model-based recognition that is concerned with how to accurately and efficiently narrow down the number of candidate models to be matched without actually searching through all the models in a database. This research features accurate and efficient target indexing in SAR images given locations of scattering centers.

In indexing, the feature correspondence and search of model database are replaced by a table look-up mechanism. This indexing table is computed off-line. A brief survey of some representative object recognition systems that have employed geometric indexing or hashing techniques is given in Table 1. Performance of these systems cannot be compared directly because they have been developed based on different assumptions. They perform in different scenarios using different features to generate object hypotheses. More importantly, it is hard to compute complex structured features from point-like features that SAR returns al-

* Corresponding author. E-mail: bhanu@engr.ucr.edu.

PII S0167-8655(96)00071-2

Table 1
State-of-the-art techniques for indexing. Approaches using structured features are marked with *.

System (year)	Acq./Recogn.	Input data	Indexing key	Comments w.r.t. SAR
Yi and Chelberg (1994)	3D/3D	range image	LSG (Local Surface Group)	*
Califano and Mohan (1994)	2D/2D	2D drawing	seven-dimensional global invariants	*
Rigoutsos and Hummel (1993)	2D/2D	intensity image	coordinates of scene points computed in the coordinate system formed by an ordered pair of scene points	point set matching (no SAR)
Beis and Lowe (1993)	2D/3D	range image	three angles and ratio of the interior edge lengths from four straight-line segment chain	*
Stein and Medioni (1992b)	2D/2D	intensity image	super segments with several different cardinalities for edges	*
Stein and Medioni (1992a)	3D/3D	range image	3D super segments with several different cardinalities for edges and splashes	*
Flynn and Jain (1992)	3D/3D	range image	two invariant feature values computed from a triple of scene surface patches that are simultaneously visible	*
Lamdan et al. (1988)	2D/2D	intensity image	coordinates of scene points in the affine-transformed coordinate system formed by an ordered triplet of three scene points	point set matching (no SAR)

though those approaches marked with asterisk (*) in Table 1 are potentially applicable to the problem of ATR from SAR images.

We have developed a computationally simple approach that efficiently retrieves correct model hypotheses when objects are represented by a pattern of point features. In the indexing table, model entries are indexed with the major axes of the patterns of scattering centers. We first index the input pattern of scattering centers using its major axis and validate candidate hypotheses using the Hausdorff distance measure. The Hausdorff distance is a method to determine the degree of resemblance between two objects when an object is represented by a set of point features. While there are other distance transforms (Paglieroni, 1992), the Hausdorff method is quite tolerant of small position errors (Huttenlocher and Kedem, 1990; Huttenlocher et al., 1993), and is reliable in the presence of noise, spurious features and some occlusion (Rucklidge, 1995). The Hausdorff distance will be described in Section 3. Using the major axis indexing, candidate hypotheses whose major axes fall within some neighborhood of the major axis computed from the input pattern are quickly retrieved. The retrieved hypotheses are then rank-ordered in the increasing order of the Hausdorff distance measure and enter the verification stage in the order they are listed. Experimental results show that indexing using major axis is very efficient and that the Hausdorff distance measure performs very well in comparing positionally noisy patterns of scattering centers, resulting in accurate retrieval of the correct model hypothesis.

Let us briefly overview our entire target object recognition system. Fig. 1 is a block diagram of the computation in the system. The entire system is divided into two parts: off-line simulation of SAR signatures of model objects and construction of indexing table and on-line recognition. In the off-line part, SAR images of target models represented by CAD files are simulated with the XPATCH software (Andersh et al., 1994) for a set of aspects (represented by *depression* and *azimuth* angles). For each image, locations of scattering centers are detected and its direction of major axis is computed. In the indexing table, model hypotheses represented by (*model name, depression angle, azimuth angle, location of scattering centers*) are linked to indexing keys that are directions of their major axes. At recognition time, scattering centers are extracted from the target chip. The major axis of the pattern of scattering centers is computed and

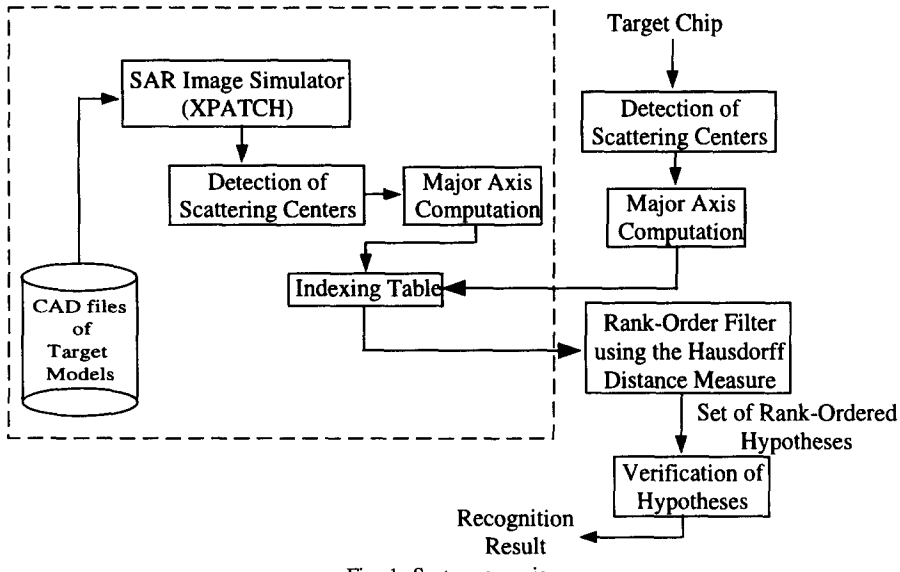

Fig. 1. System overview.

models whose major axis is within $\pm\varepsilon^\circ$ (threshold) neighborhood of the input major axis are quickly collected from the indexing table. At this stage, we apply the Hausdorff distance measure to match the scattering centers of the models and the target chip so as to validate the candidate hypotheses. We rank-order these hypotheses in the ascending order of Hausdorff distance and they enter the verification stage in the order they are listed. A metric is used here to verify the hypotheses for correct recognition result.

The contribution of this work is an efficient and accurate model retrieval method for target recognition in SAR images using a combination of the major axis analysis and the Hausdorff distance measure.

The following section presents the method to compute the major axis using the principal component analysis. Section 3 briefly describes the Hausdorff distance measure. Finally, Section 4 reports experimental results for our current model database consisting of four armored vehicle targets, FRED, T72, T80 tanks and SCUD missile launcher.

2. Computing major axis

We employed the principal component analysis to compute the major axis of a pattern of scattering centers. Principal component analysis is a well-known exploratory data analysis and is frequently used to reduce the dimensionality of a data set and extract new features from the original data which are uncorrelated. The use of this technique is specialized to two dimensions in this work, however, it can be used with input data of any dimensionality.

Assume that the input data is expressed as a matrix $\boldsymbol{X}$ with each row i containing the coordinates of one of the scattering centers $\boldsymbol{x}_i = (x_i, y_i)$:

$$\boldsymbol{X} = \begin{bmatrix} x_1 & y_1 \\ \vdots & \vdots \\ x_n & y_n \end{bmatrix}.$$

The following steps are performed using this input matrix:

Step 1. The sample mean is computed for x and y coordinates as $\hat{\mu}_x = (1/n)\sum_{i=1}^{n} x_i$ and $\hat{\mu}_y = (1/n)\sum_{i=1}^{n} y_i$, respectively. A centered data matrix $\boldsymbol{X}^*$ is constructed from $\boldsymbol{X}$:

$$\boldsymbol{X}^* = \begin{bmatrix} x_1 - \hat{\mu}_x & y_1 - \hat{\mu}_y \\ \vdots & \vdots \\ x_n - \hat{\mu}_x & y_n - \hat{\mu}_y \end{bmatrix}.$$

Step 2. The sample covariance matrix $\hat{\boldsymbol{R}} = (1/n)[\boldsymbol{X}^*]^{\mathrm{T}}\boldsymbol{X}^*$ is obtained and its eigensystem is computed, yielding two eigenvalue and eigenvector

pairs $\{(v_1, \lambda_1), (v_2, \lambda_2)\}$. Assume that the two pairs are sorted so that $\lambda_1 \geqslant \lambda_2$.

The two eigenvectors, v_1 and v_2, span the 2D imaging plane and the eigenvector v_1 is the direction in the plane along which the data's sample variance is the larger (λ_1 is the sample variance along the direction). v_2 is the direction orthogonal to v_1 with the larger variance. The directionality of v_i is an excellent estimate of the orientation of a scattering pattern. To resolve the 180° ambiguity, we use the direction that forms an acute angle with x axis as the direction of major axis.

3. The Hausdorff distance measure

Given two finite point sets $A = \{a_1, \ldots, a_p\}$ and $B = \{b_1, \ldots, b_q\}$, the Hausdorff distance is defined as

$$H(A, B) = \max(h(A, B), h(B, A)), \tag{1}$$

where

$$h(A, B) = \max_{a \in A} \min_{b \in B} \|a - b\| \tag{2}$$

and $\|\cdot\|$ is some underlying norm on the points of A and B.

Fig. 2 illustrates the Hausdorff distance using two sets, A and B, consisting of two points. The function $h(A, B)$ is called the *directed* Hausdorff distance from A to B. It identifies the point $a \in A$ that is farthest from any point of B and measures the distance from a to its nearest neighbor in B (using the given norm $\|\cdot\|$), that is, $h(A, B)$ in effect ranks each point of A based on its distance to the nearest point of B and then uses the largest ranked such point as the distance (the most mismatched point of A). Point of A must be within distance d of some points of B, and also there is some point of A that is exactly distance d from the nearest point of B (the most mismatched point). The Hausdorff distance $H(A, B)$ is the maximum of $h(A, B)$ and $h(B, A)$. Thus, it measures the degree of mismatch between two sets by measuring the distance of the point of A that is farthest from any point of B and vice versa. The notion of resemblance encoded by this distance measure is that each member of A be near some member of B and vice versa. Unlike most methods of comparing shapes, there is no explicit pairing of points of A with points of B (for example, many points of A may be close to the same point of B). The function $H(A, B)$ can be trivially computed in time $O(pq)$ for two point sets of size p and q, respectively, and this can be improved to $O((p + q)\log(p + q))$ (Alt et al., 1991). Note that there are several modifications of the Hausdorff distance (Rucklidge, 1995). We have used the most common definition since it is suited for our problem.

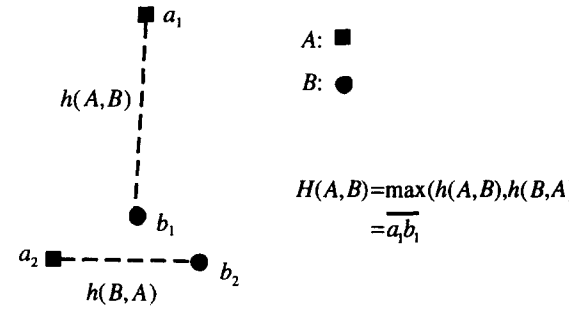

Fig. 2. An illustration of the Hausdorff distance.

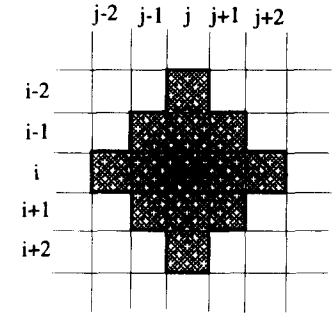

Fig. 3. Local neighborhood (filled region) that is used to detect scattering centers.

4. Experimental results

The current model database includes four armored vehicle targets, FRED tank, T72 tank, T80 tank and SCUD missile launcher. The radar signature predictions (at six inch resolution for all azimuths from 0° to 359° in 1° steps at 15° elevation) of these vehicle targets are generated using the XPATCH SAR simulation code. We use a total of 1440 images to build the model base, and use 2880 images to test the performance of our indexing approach.

Note that the intensity noise originally generated from SAR imaging is called *speckle* noise and it is a multiplicative type of noise. The intensity value that

is logarithmically transformed is used for the interpretation of SAR data. Therefore, the noise of the logarithmically transformed intensity image can be approximated by additive Gaussian noise (Arsenault and April, 1976). We assumed (see below) that positional uncertainty of the scattering center is approximately Gaussian.

We employ the following method to detect scattering centers. Other, more complicated, methods can be used, as long as they produce locations of scattering centers. We consider current pixel location a candidate scattering center if the magnitude of SAR return at the current pixel is a local maximum in the local neighborhood shown in Fig. 3. Current pixel location is considered a local maximum if the following four conditions are met:

$$\begin{aligned}
&z(i,j-2) < z(i,j-1) < z(i,j) \\
&\quad > z(i,j+1) > z(i,j+2), \\
&z(i-2,j) < z(i-1,j) < z(i,j) \\
&\quad > z(i+1,j) > z(i+2,j), \\
&z(i-1,j-1) < z(i,j) > z(i+1,j+1), \\
&z(i-1,j+1) < z(i,j) > z(i+1,j-1), \qquad (3)
\end{aligned}$$

where $z(i,j)$ represents the magnitude of the image at the current pixel location, (i,j). The same method is used for detection of scattering centers during both off-line and on-line processes. Examples of scattering centers detected using this method and major axes computed from these scattering centers are shown in Fig. 4 for the four vehicle targets at azimuth angle 18°. Corresponding target signatures are shown on the left side. For each image, top twenty scattering centers in terms of magnitude are selected in these experiments. If the number of scattering centers is less than twenty, all available scattering centers are used. After all scattering centers are identified, an indexing table is built where a model entry (*model name, depression angle, azimuth angle, locations of scattering centers*) is linked to a leaf node of the binary tree that spans a small range (ε) of directions containing the major axis direction of the entry.

We have used two sets of test data. One set of data is non-occluded data (1440 images) and the other is occluded data (1440 images). The occluded data can be considered a bad real noisy situation. Data for all azimuth angles from 0° to 359° are used as test data. To create the occluded data, we have cut 10% of each image from the right side. We add positional noise to locations of scattering centers of non-occluded data and occluded data. We generate noisy locations of scattering centers, $(x + N_1(0,\sigma^2), y + N_2(0,\sigma^2))$, using two Gaussian random noise generators, N_1 and N_2. (x,y) is a noiseless location of a scattering center and $N(0,\sigma^2)$ denotes Gaussian noise of mean 0 and standard deviation σ. We have employed a rather strict requirement for a successful indexing because we want a correct hypothesis to appear early in the candidate list from the rank-order filter using the Hausdorff distance measure. We consider an indexing result correct only when the first model entry ordered by the Hausdorff distance measure is the same as the input. This is the metric for correct indexing result that we use for the experiments reported in this paper. Figs. 5(a) and (b) show the indexing performance of our method for non-occluded data and occluded data, respectively, as the amount of positional noise added to location of scattering centers varies. In the case of non-occluded data, we have found that correct hypotheses were always in the candidate list. As expected, the result shows that we need to use a larger value of $\varepsilon°$ to retrieve model hypotheses when noise gets large. As can be seen in Fig. 5(a), for 90% of the time, in the case of $\varepsilon = 5°$, the first entry in the ordered list was the correct hypothesis. For the occluded data, for 80% of the time, in the case of $\varepsilon = 5°$, the first entry in the ordered list was the correct hypothesis. Even though the amount of noise increases, the accuracy of indexing does not degrade significantly.

5. Conclusions

We have proposed an efficient method to retrieve object hypotheses using the major axis indexing and the Hausdorff distance measure. The major axis indexing technique efficiently narrows down the number of candidate hypotheses. The Hausdorff distance measure performs well in picking the correct hypothesis and is quite tolerant of positional errors in locations of scattering centers. These properties of the algorithm along with computational efficiency make the proposed method a promising approach to target indexing in SAR images and suggest that further evaluations with real SAR imagery are warranted.

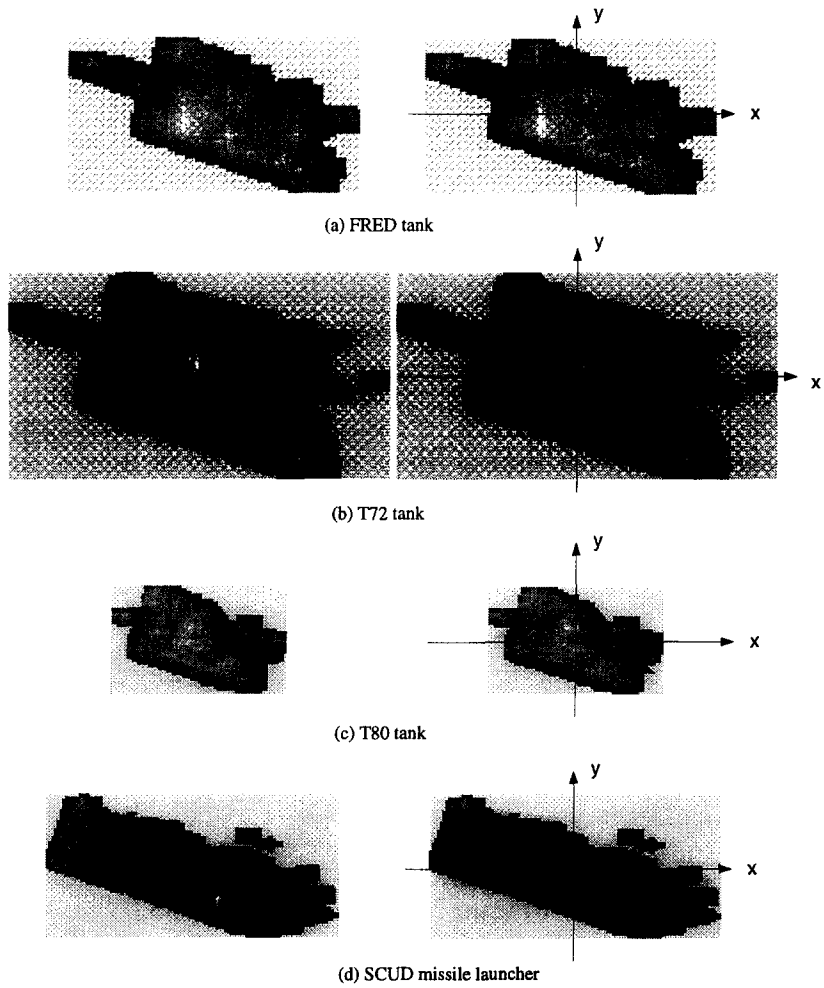

Fig. 4. Magnitude of SAR returns (left) and scattering centers marked with small dark squares (right) for (a) FRED tank, (b) T72 tank, (c) T80 tank and (d) SCUD missile launcher (down) at azimuth angle 18° and elevation angle 15°. Only the target region taken from a 256 × 256 target chip (6" resolution) is shown, and it is zoomed in for clear visualization of scattering centers on the target. The original sizes of images in (a), (b), (c) and (d) are 85 × 45, 111 × 60, 60 × 40 and 110 × 54, respectively.

Acknowledgments

This work was supported by ARPA Grant number MDA972-93-1-0010. The synthetic SAR data used in this work were generated by Grinnell Jones.

References

Special issue on automatic target recognition (1993). *The Lincoln Laboratory J.* 6 (1).

Alt, E., B. Behrends and J. Blomer (1991). Measuring the resemblance of polygonal shapes. *Proc. Seventh ACM Symp. on Computational Geometry*, 1991.

Andersh, D.J., S.W. Lee, H. Ling and C.L. Yu (1994). Xpatch: a high frequency electromagnetic scattering prediction code using shooting and bouncing ray. *Proc. Ground Target Modeling and Validation Conf.*, August 1994, 498–507.

Arsenault, H.H. and G. April (1976). Properties of speckle integrated with a finite aperture and logarithmically transformed. *J. Opt. Soc. Amer.* 66, 1160–1163.

Beis, J. and D. Lowe (1993). Learning indexing functions for 3-D model-based object recognition. *AAAI Workshop*, April 1993.

Bhanu, B., G. Jones, J. Ahn, M. Li and J. Yi (1996). Recognition of articulated targets in SAR images. *Proc. ARPA Image Understanding Workshop*, Palm Springs, CA, February 1996, Vol. 2, 1237–1250.

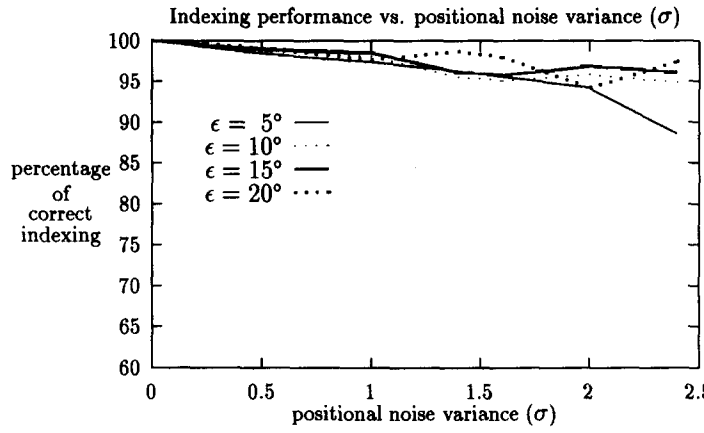

(a)

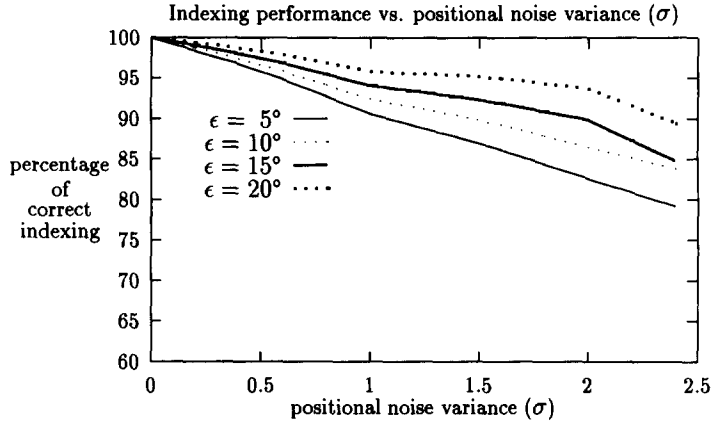

(b)

Fig. 5. Indexing performance of the algorithm as the amount of positional noise varies: for (a) non-occluded test data and (b) 10% occluded test data. Models whose major axis is within $\varepsilon°$ (threshold) neighborhood of the input major axis are quickly collected from the indexing table. Indexing is considered successful when the first entry of the set of rank-ordered hypotheses list is the correct answer.

Califano, A. and R. Mohan (1994). Multidimensional indexing for recognizing visual shapes. *IEEE Trans. Pattern Anal. Mach. Intell.* 16 (4), 373–392.

Dudgeon, D.E., R.J. Lacoss, C.H. Lazott and J.G. Verly (1994). Use of persistent scatterers for model-based recognition. *SPIE* 2230, 356–368.

Fitch, J.P. (1988). *Synthetic Aperture Radar*. Springer, New York.

Flynn, P. and A.K. Jain (1992). 3d object recognition using invariant feature indexing of interpretation tables. *Comput. Vision Graphics Image Process.: Image Understanding* 55 (3), 119–129.

Huttenlocher, D.P. and K. Kedem (1990). Efficiently computing the Hausdorff distance for point sets under translation. *Proc. Sixth ACM Symp. on Computational Geometry*, 1990.

Huttenlocher, D.P., G.A. Klanderman and W.J. Rucklidge (1993). Comparing the images using the Hausdorff distance. *IEEE Trans. Pattern Anal. Mach. Intell.* 15 (9), 850–863.

Lamdan, Y., J. Schwartz and H. Wolfson (1988). Object recognition by affine invariant matching. *Proc. IEEE Conf. on Computer Vision and Pattern Recognition*, Ann Arbor, MI, June 1988, 335–344.

Novak, L.M., G.J. Owirka and C.M. Netishen (1993). Performance of a high-resolution polarimetric SAR automatic target recognition system. *The Lincoln Laboratory J.* 6 (1), 11–24.

Paglieroni, D.W. (1992). Distance transforms: properties and machine vision applications. *Comput. Vision Graphics Image Process.* 54, 156–174.

Rigoutsos, I. and R. Hummel (1993). Distributed Bayesian object recognition. *Proc. IEEE Conf. on Computer Vision and Pattern*

Recognition, New York City, NY, June 1993, 180–186.

Rucklidge, W.J. (1995). Locating objects using the Hausdorff distance. *Proc. 5th Internat. Conf. on Computer Vision*, Cambridge, MA, 20–23 June 1995, 457–464.

Stein, F. and G. Medioni (1992a). Structural indexing: Efficient 3-D object recognition. *IEEE Trans. Pattern Anal. Mach. Intell.* 14 (2), 125–145.

Stein, F. and G. Medioni (1992b). Structural indexing: Efficient 2-D object recognition. *IEEE Trans. Pattern Anal. Mach. Intell.* 14 (12), 1198–1204.

Waxman, A.M., M. Seibert, A.M. Bernardon and D.A. Fay (1993). Neural systems for automatic target learning and recognition. *The Lincoln Laboratory J.* 6 (1), 77–116.

Yi, J.H. and D.M. Chelberg (1994). Rapid obeject recognition from a large model database. *Proc. 2nd IEEE CAD-Based Workshop*, Champion, PA, 1994, 28–35.